

SUPPLEMENTARY INFORMATION

Augmenting the efficacy of chemotherapies by inhibiting the Gas6/Axl pathway

Mihalis S. Kariolis^{1*}, Yu Rebecca Miao^{1*}, Anh Diep¹, Shannon E. Nash¹, Monica M. Olcina¹, Dadi Jiang¹, Douglas S. Jones II², Shiven Kapur², Irimpan I. Mathews³, Albert C. Koong¹, Erinn B. Rankin¹, Jennifer R. Cochran^{2†}, Amato J. Giaccia^{1†}

Affiliations:

¹ Department of Radiation Oncology, Stanford University School of Medicine, Stanford University, Stanford, California 94305, USA

² Department of Bioengineering, Stanford University, Stanford, California 94305, USA

³ Stanford Synchrotron Radiation Lightsource, SLAC National Accelerator Laboratory, 2575 Sand Hill Road MS 99, Menlo Park, California 95124, USA

* M. S. Kariolis and Y. R. Miao contributed equally to this work.

† Corresponding authors.

Amato J. Giaccia (A.J.G.)
CCSR-South, Room 1255,
269 Campus Drive
Stanford, CA 94305-5152

Phone: 650.723.7311

Email: giaccia@stanford.edu

Jennifer R. Cochran (J.R.C)
Shriram Center for Bioengineering and Chemical Engineering
443 Via Ortega, Room 356
Stanford, CA 94305-4125
Phone: 650.724.5034
Email: cochran@stanford.edu

Supplementary tables

Table S1: In-depth sequencing of enriched Axl Ig1 library pools §

Clone	19	23	26	27	32	33	38	44	61	65	72	74	78	79	86	87	88	90	92	97	98	105	109	112	113	116	118	127	129	# of repeats
wt	A	T	E	E	G	N	T	T	H	D	A	S	Q	V	Q	D	D	I	V	I	T	T	Q	V	F	H	T	G	G	
MYD1					S						V					G												R		62
MYD2			G											M														E		21
MYD3						S						N				G														1
MYD4											V											R				R				1
MYD5																														16
MYD6													E																	1
MYD7											V																			7
MYD8															R			V												10
MYD9											V																			1
MYD10										N						G														1
MYD11																G														2
MYD12				K					Y		V						N				A		A							1
MYD13																							R							1
MYD14								A			V							V					M					K		1
MYD15																														2
MYD16																									A	L		A		1
MYD17																						P								1
MYD18				G												G														1
MYD19							I																							2
MYD20																G														3
MYD21		M																												1
MYD22											V																L			1
MYD23															R															1
MYD24	T		G	G																										1
MYD25																		M												1
																TOTAL:											141			

§ 38 of these sequences were previously reported in Kariolis *et al* (17). An additional 103 clones were sequenced at random from the pool of Axl mutants recovered from sort 5. These two data sets were combined into Table S1 above. The residue number is listed at the top and the corresponding wild-type amino acid is given. The frequency of each clone is listed in the right hand column. Three mutations were prevalent: A72V, D87G, and V92A. Each was found as a single point mutant, as well as in combination with other mutations.

Table S2

	Gas6 binding and thermodynamic parameters				
	K_d (fM) hGas6 *apparent	k_{on} ($10^7 M^{-1}s^{-1}$)	k_{off} ($10^{-5} s^{-1}$)	ΔG° (kcal/mol)	$\Delta\Delta G^\circ$ to wt Axl
A72V Ig1	$5,800 \pm 100$	1.9 ± 0.04	11.0 ± 0.2	-15.32	-1.03
MYD1-72 Ig1	720 ± 10	1.7 ± 0.05	1.2 ± 0.4	-16.56	-2.27
MYD1-72 Fc	$*93 \pm 1$	2.7 ± 0.08	0.25 ± 0.00		

Binding affinities of the Axl A72V variants, and apparent binding affinity of MYD1-72 Fc. On-rates were directly measured using the KinExA, while off-rates were calculated as a ratio of the K_d and k_{on} .

Table S3: Crystallographic statistics for the Gas6/MYD1-72 co-complexes

	Gas6/MYD1-72 Active co-complex (2:2)	Gas6/MYD1-72 Truncated complex (1:1)
Crystallographic parameters		
Space group	P3 ₂ 21	P2 ₁ 2 ₁ 2 ₁
Unit-cell parameters		
a, b, c (Å)	113.04, 113.04, 361.86	77.22, 80.47, 249.65
α , β , γ (°)	90, 90, 120	90, 90, 90
Data collection statistics		
Resolution limits (Å)	38.15 - 3.50	38.61 – 2.30
Number of observed reflections	244258	749622
Number of unique reflections	33726	69824
Completeness (%)		
overall / outer shell	96.6 / 91.0	99.6 / 97.9
Redundancy		
overall / outer shell	7.2 / 3.4	10.7 / 4.1
R _{sym} (%)		
overall / outer shell	13.6 / 74.4	7.2 / 101.3
I/ σ		
overall / outer shell	11.1 / 1.6	20.1 / 1.7
Refinement statistics		
Resolution limits (Å)	38.15 - 3.50	38.61 – 2.30
Number of reflections (%)	31985 (96.6)	66331 / 99.6
Reflections used for R _{free}	1684	3492
R _(working) (%)	20.3	19.8
R _{free} (%)	24.5	24.7
Model contents/average B (Å) ²		
Protein atoms (includes sugars)	8905 / 114.7	7503 / 32.7
Ions	14 / 141.2	4 / 64.3
Water molecules	3 / 76.2	189 / 48.6
Ramachandran plot (%)		
favored / outliers	93.28 / 1.15	96.6 / 0.64
RMS deviations		
Bond length (Å)	0.007	0.018
Bond angle (°)	1.247	1.996

Table S5: Doses of clinical TKIs

Compound	Trade name	Recommended daily dose (mg)	~ mg/kg 70 kg patient
Afatinib	Gilotrif	40	0.57
Axitinib	Inlyta	5	0.07
Bosutinib	Bosulif	600	8.57
Cabozantinib	Cometriq	140	2.00
Ceritinib	Zykadia	750	10.71
Crizotinib	Xalkori	500	7.14
Dabrafenib	Tafinlar	300	4.29
Dasatinib	Sprycel	140	2.00
Erlotinib	Tarceva	150	2.14
Gefitinib	Iressa	250	3.57
Ibrutinib	Imbruvica	560	8.00
Idelalisib	Zydelig	300	4.29
Imatinib	Gleevec	800	11.43
Lapatinib	Tykerb	1500	21.43
Lenvatinib	Lenvima	24	0.34
Nilotinib	Tasinga	800	11.43
Olaparib	Lynparza	800	11.43
Palbociclib	Ibrance	125	1.79
Pazopanib	Votrient	800	11.43
Regorafenib	Stivarga	160	2.29
Ruxolitinib	Jakafi	50	0.71
Sonidegib	Odomzo	200	2.86
Sorafenib	Nexavar	800	11.43
Sunitinib	Sutent	50	0.71
Trametinib	Mekinist	2	0.03
Vandetanib	Caprelsa	300	4.29
Vemurafenib	Zelboraf	1812	25.89
Vismodegib	Erivedge	150	2.14

Recommended daily doses were taken from the FDA labels from each of the approved molecules. For those compounds for which twice daily doses were recommended, the cumulative daily dose is listed. The approximate mg/kg equivalent was calculated assuming an average patient weight of 70 kg.

Supplementary Figures

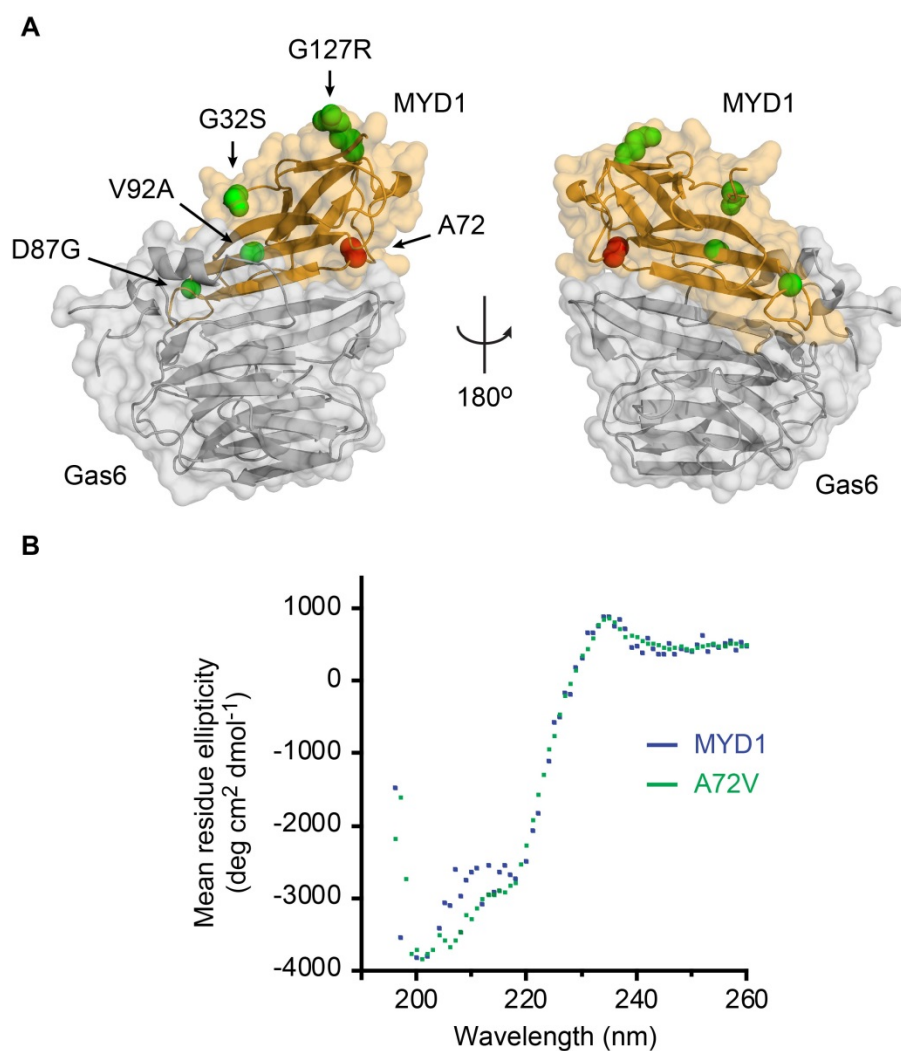


Figure S1: Structural rationale for combining MYD1 and A72V. (A) The major binding interaction between MYD1 Ig1 (orange) and Gas6 LG1 (gray) is shown. Side chains of the four mutations in MYD1 are shown in green spheres while A72 is shown in red spheres to indicate its relative position. (B) The far UV circular dichroism spectra of MYD1 Ig1 and A72V Ig1 at 20 °C are overlaid, demonstrating the similarities in the secondary structure of these proteins. These scans suggest that A72V is not disruptive to the structure of the Axl Ig1 domain.

Figure S2: *Kinetic exclusion assay data for experiments performed on Axl A72V variants.* (A) N-curve analysis of Gas6 equilibrium binding titrations measured by KinExA for A72V Ig1, MYD1-72 Ig1 and MYD1-72 Fc. Titrations using concentrations lower than 15 pM Gas6 were not used as robust signal-to-noise could not be obtained below this level. (B) Direct inject kinetic data to determine the k_{on} of binding interactions. Curve fits are shown as dotted black lines, and nominal Gas6 concentrations are given. For quantification, see Supplementary Table 2. (C) Thermodynamic cycle analysis shows the differences in the free energy of binding to Gas6 between wild-type Axl, A72V, MYD1, and MYD1-72. $\Delta\Delta G^0$ values are expressed in kcal/mol.

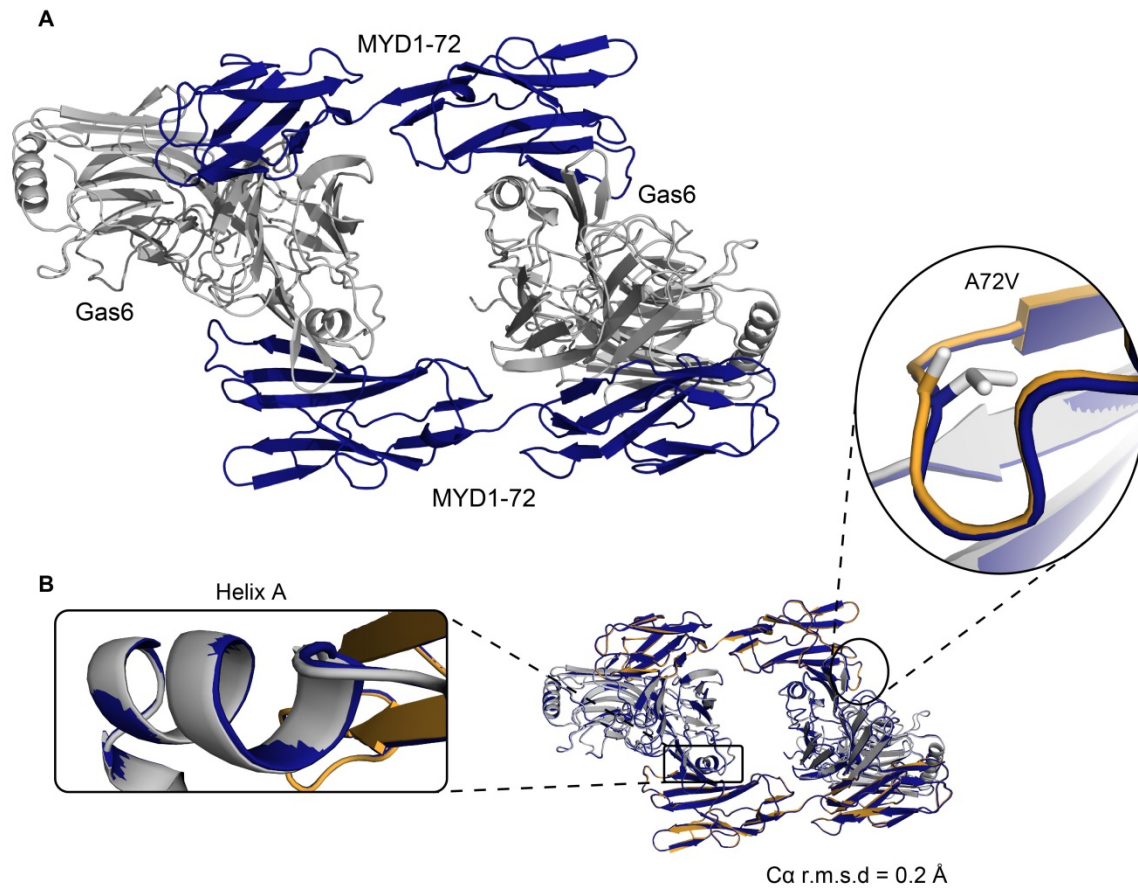


Figure S3: *Structural analysis of the Gas6/MYD1-72 2:2 co-complex.* (A) Gas6/MYD1-72 co-complex showing the overall geometry and 2:2 stoichiometry of the active complex. Gas6 is shown in gray with MYD1-72 is in blue. The co-complex consists of two copies each of Gas6 LG1-2 and MYD1-72 Ig1-2. (B) Overlay of the Gas6/MYD1 (grey/orange) and Gas6/MYD1-72 (blue) co-complex structures. No significant changes were observed between the two structures (r.m.s.d. 0.2 Å). In particular, there were no deviations within the loop containing residue 72, or on Helix A on Gas6.

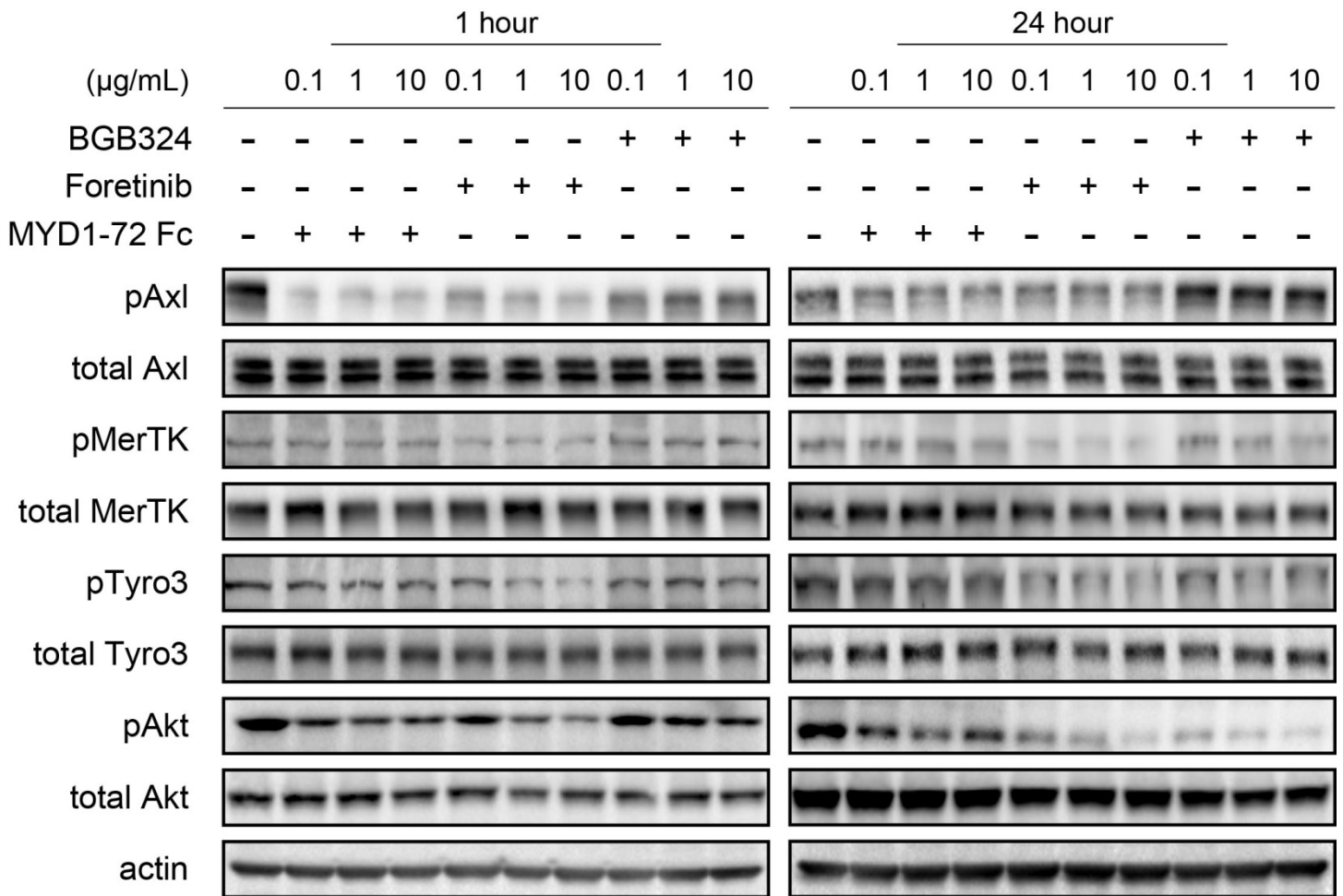


Figure S4: *In vitro* analysis of MYD1-72 Fc and TKI activity. (A) OVCAR8 ovarian cancer cells were treated with 0.1, 1, or 10 $\mu\text{g/mL}$ of BGB324, Foretinib, or MYD1-72 Fc for 1 or 24 hours. Activation of all three TAM family receptors as well as downstream Akt activation was monitored.

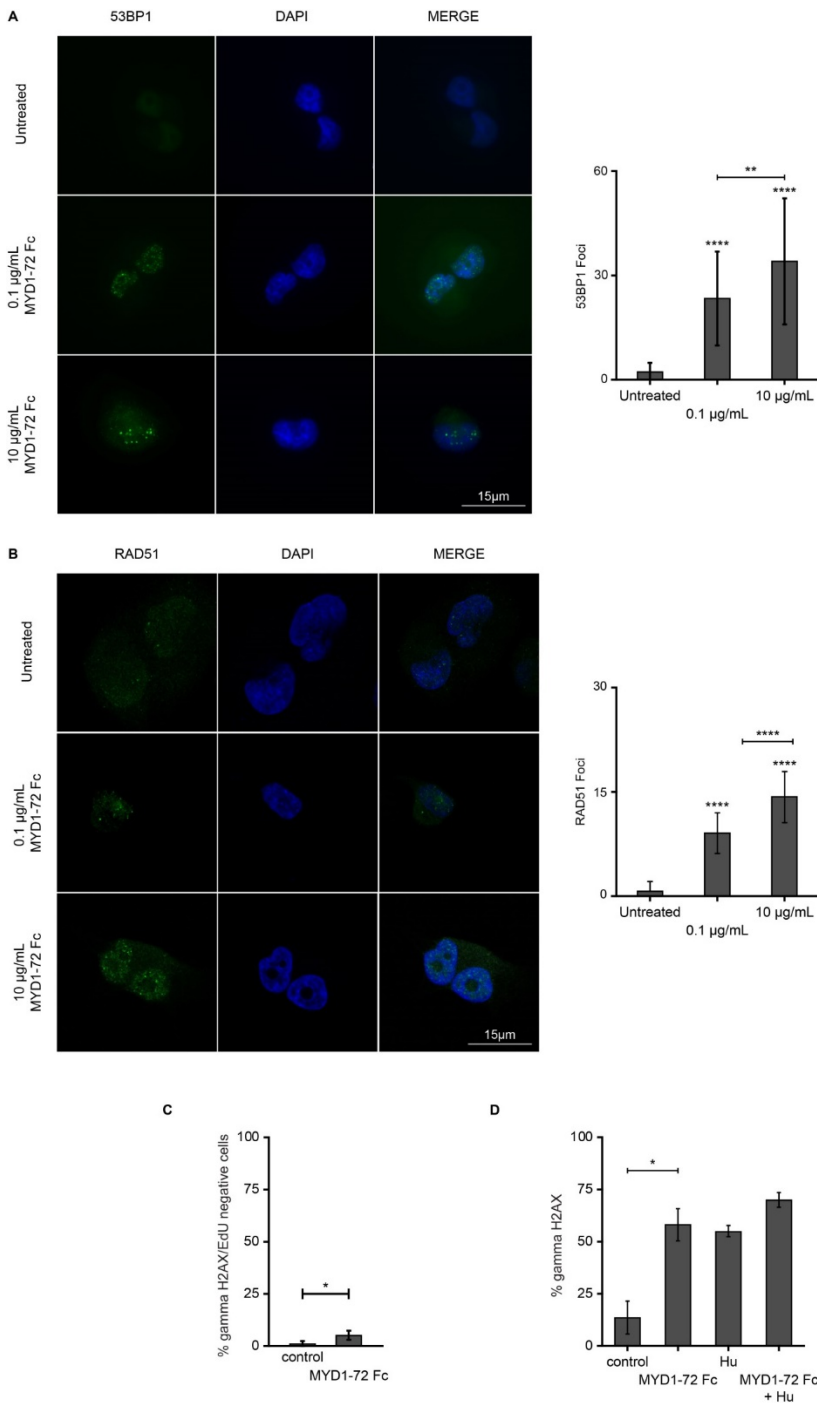


Figure S5: MYD1-72V Fc induces DNA damage response. (A) Immunofluorescence staining detecting 53BP1 foci formation in OVCAR8 cells treated with 0.1 and 10µg/ml of MYD1-72 Fc indicative of non-homologous end joining (NHEJ) for cells in G1 phase. (B) Immunofluorescence staining detecting RAD51 foci formation in OVCAR8 cells treated with 0.1 and 10µg/ml of MYD1-72 Fc as a marker of homologous recombination (HR) for cells in S phase. (C) The percentage of γ H2AX positive cells that are in non S-phase cells (EdU negative) between control and MYD1-72 Fc treated groups. (D) The number of γ H2AX positive cells (either as pan nuclear staining or in foci) counted following different treatments, including MYD1-72 Fc, hydroxyurea (Hu) and MYD1-72 Fc and Hu is shown. For Hu treated groups, γ H2AX positive cells refers to cells where a pan-nuclear staining pattern (typically associated with replication stress) was observed, as a 6 hours Hu treatment is expected to result in replication stress in the absence of DNA breaks. Average counts from three independent experiments are shown in each graph. Error bars represent \pm stdev, * $P < 0.05$, **** $P < 0.0001$.

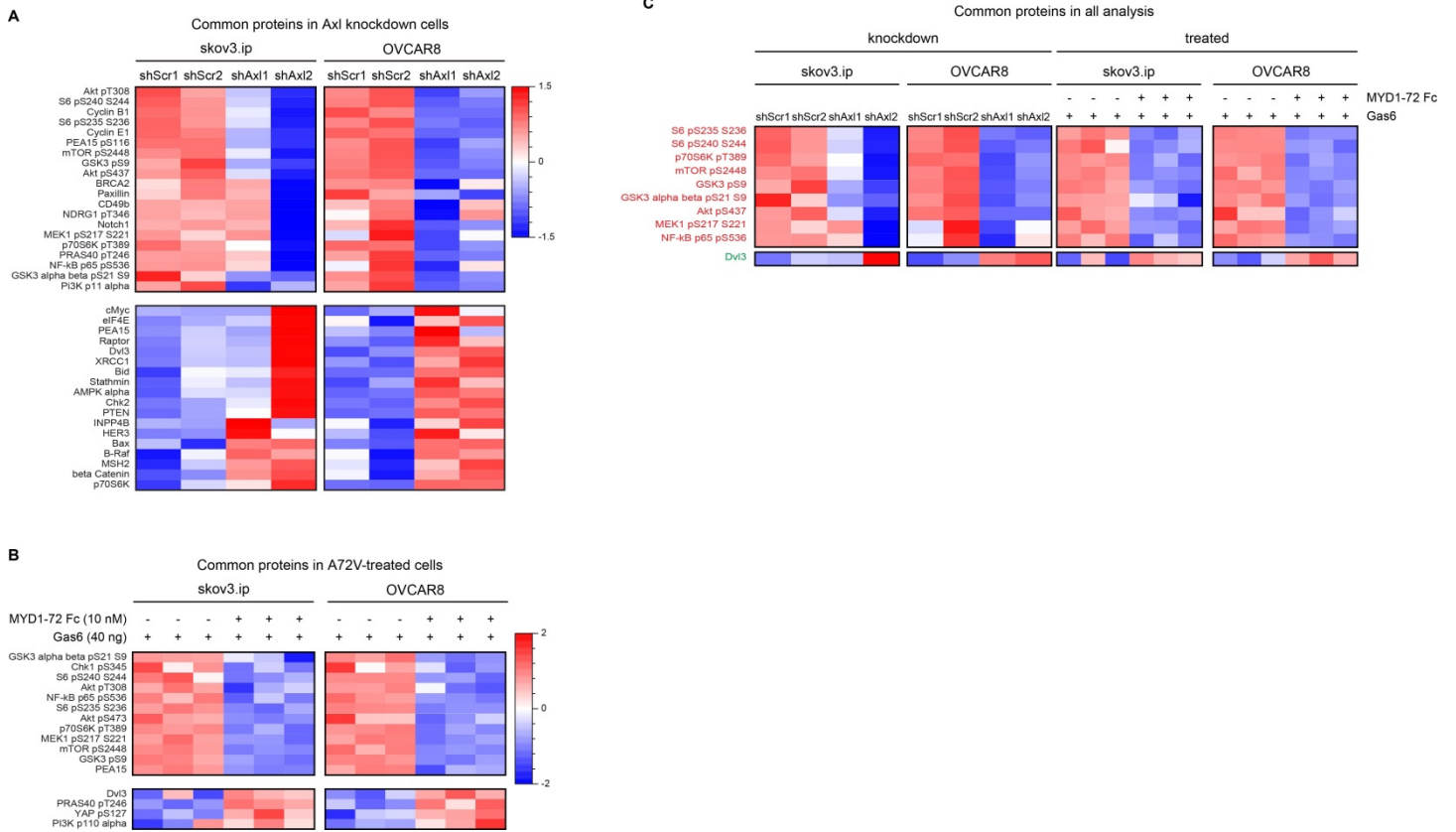


Figure S6: Reverse phase protein array (RPPA) of Axl knockdown and MYD1-72 Fc treated cells. Proteins differentially expressed between shAxl and shScr cells (A), MYD1-72 Fc and saline treated cells (B), or common proteins across both data sets (C). Only those proteins that were found to be similarly altered in both cell lines are shown.

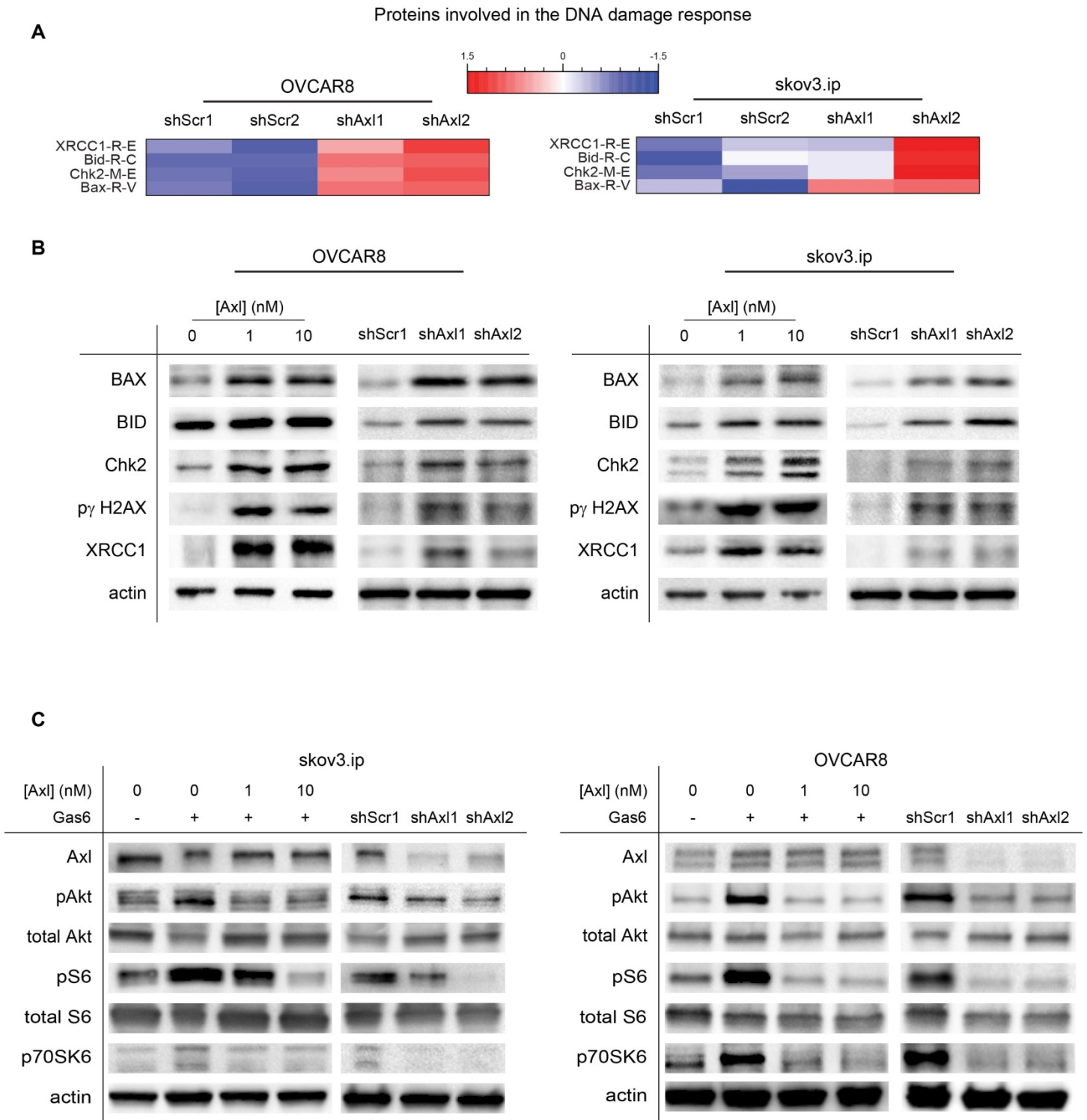


Figure S7: Axl inhibition alters the cellular response to DNA damage. (A) Heat map of proteins related to the DNA damage response found to be differentially regulated upon Axl inhibition. (B) Western blots confirming the results of the RPPA. Expression of proteins involved in the DNA damage response was altered when Axl was knocked down by shRNA, or pharmacologically inhibited using MYD1-72 Fc. (C) Western blot confirmation of several proteins involved in EMT, which were commonly downregulated in both knockdown and treated samples.

skov3.ip

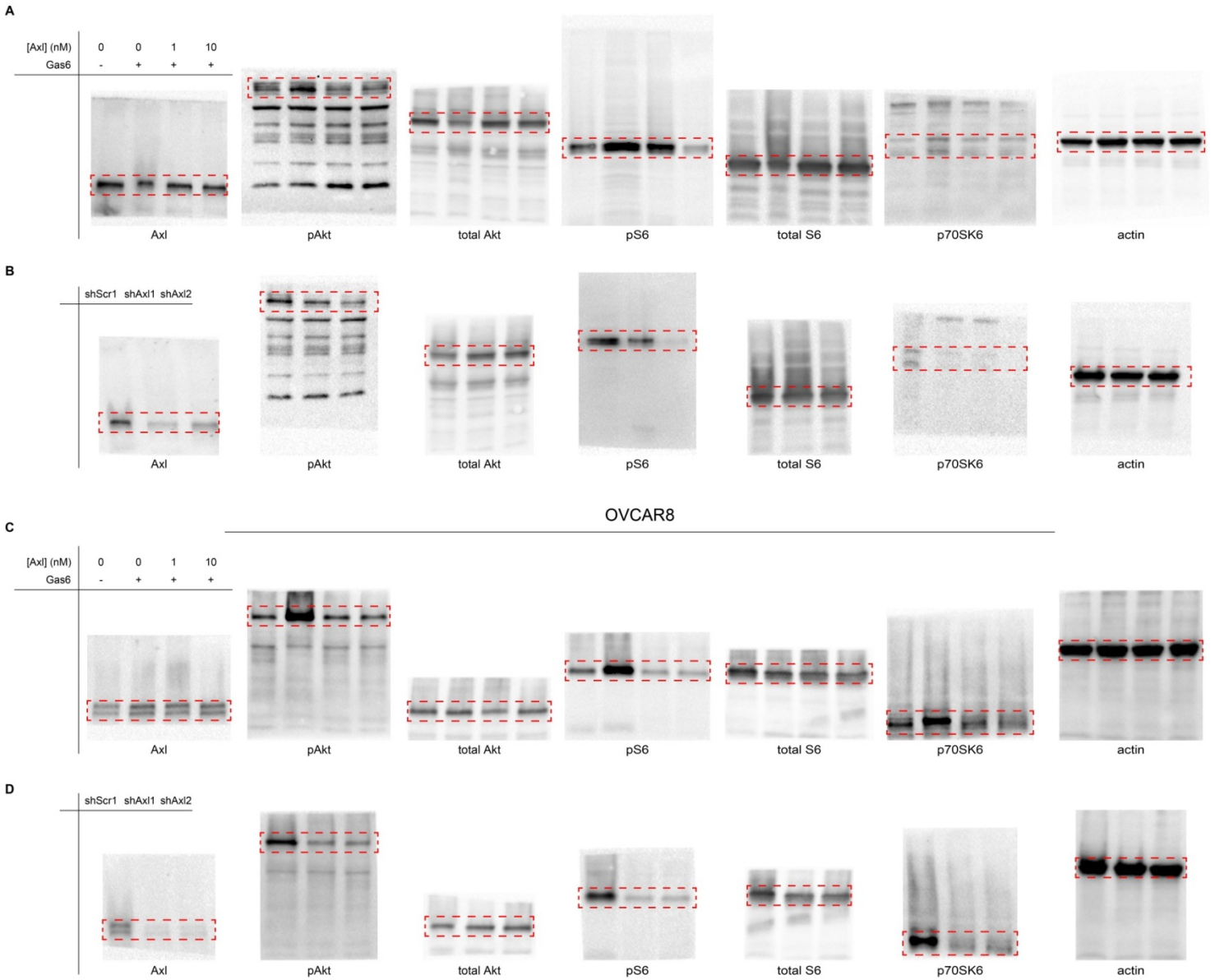


Figure S8: *Uncropped western blots from Figure S7.* Blots were performed on lysate from skov3.ip (A, B) and OVCAR8 (C, D) ovarian cancer cells either treated with MYD1-72 Fc (A, C) or from shAxl lines (B, D). Red boxes indicate the region cropped for display in Figure S7.

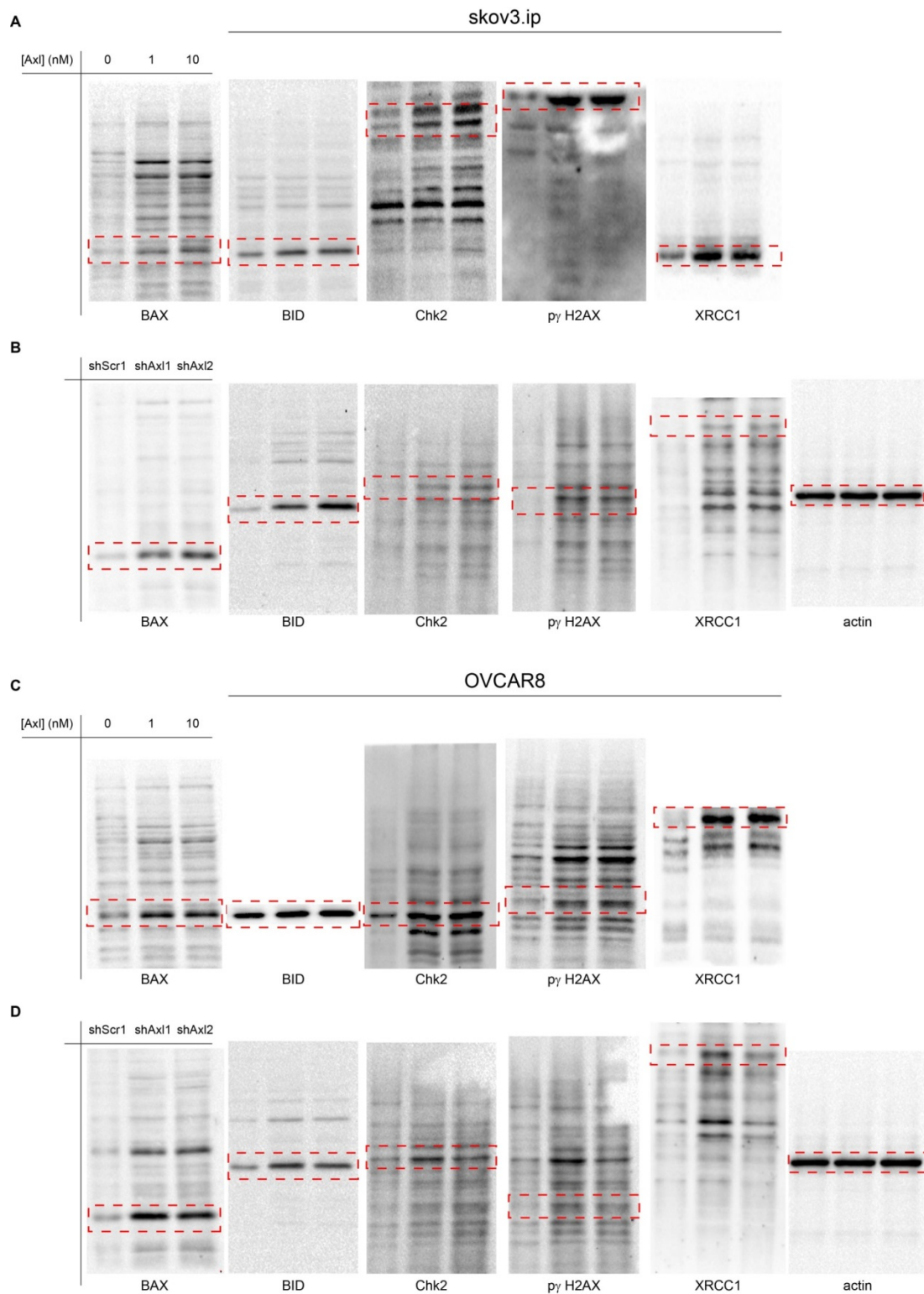


Figure S9: *Uncropped western blots from Figure S7.* Blots were performed on lysate from skov3.ip (A, B) and OVCAR8 (C, D) ovarian cancer cells either treated with MYD1-72 Fc (A, C) or from shAxl lines (B, D). Red boxes indicate the region cropped for display in Figure S7.